# Electronic Supplementary Information

# A high-throughput microfluidic single-cell screening platform capable of selective cell extraction

**Hyun Soo Kim[a], Timothy P. Devarenne[b], and Arum Han[a, c*]**

[a] Department of Electrical and Computer Engineering, Texas A&M University, College Station, Texas 77843, USA

[b] Department of Biochemistry and Biophysics, Texas A&M University, College Station, Texas 77843, USA

[c] Department of Biomedical Engineering, Texas A&M University, College Station, Texas 77843, USA

[*]Correspondence should be addressed to Arum Han (arum.han@ece.tamu.edu).

| | |
|---|---|
| **Supplementary Information** | Microfabricated high-throughput screening platform |
| | Numerical simulation of three different trapping site designs |
| **Supplementary Fig. S1** | Optical profilometer measurement of the fabricated devices |
| **Supplementary Fig. S2** | Success rate of the selective cell extraction process |
| **Supplementary Fig. S3** | Cell viability test after the selective cell extraction process |
| **Supplementary Video S1** | 3D structure of a single trapping site with a captured *C. reinhardtii*, reconstructed by confocal microscopy (yellow: Nile red stained PDMS device, red: chlorophyll autofluorescence of *C. reinhardtii*) |
| **Supplementary Video S2** | Operation of the microfluidic OR logic gate (middle control |

| | |
|---|---|
| | layer actuation only) |
| **Supplementary Video S3** | Operation of the microfluidic OR logic gate (top control layer actuation only) |
| **Supplementary Video S4** | Operation of the microfluidic OR logic gate (both the top and middle control layers being actuated) |
| **Supplementary Video S5** | Operation of the microfluidic OR logic gate, showing the selection of a particular trapping site (in this case, the left bottom trapping site first, followed by the right top trapping site) from a 2 x 2 array trapping array |
| **Supplementary Video S6** | Time-course analysis of a single *C. reinhardtii* cell growth inside a trapping site of the microfluidic platform. |
| **Supplementary Video S7** | Sequential selective cell extractions from three different trapping sites |

# Supplementary Information

## Microfabricated high-throughput screening platform

The single-cell screening platform was successfully fabricated by replicating each PDMS layer (the top control layer, the middle control layer, and the bottom cell culture/analysis layer) from the mater molds and assembling all the layers together (SI Fig. S1A-C). Compared to our model microalga, *C. reinhardtii* (typical diameter: 5 ~ 10 μm), the trapping structure has a slightly larger opening (15 μm) at the front, where single microalgal cells could be successfully captured. The 3D structure of the single trapping site with a captured *C. reinhardtii* is shown in SI Fig. S1D, reconstructed using confocal microscopy by intentionally over-staining the PDMS device with Nile red to view the trapping structure and using chlorophyll autofluorescence to view the *C. reinhardtii* cell (Supplementary Video S1).

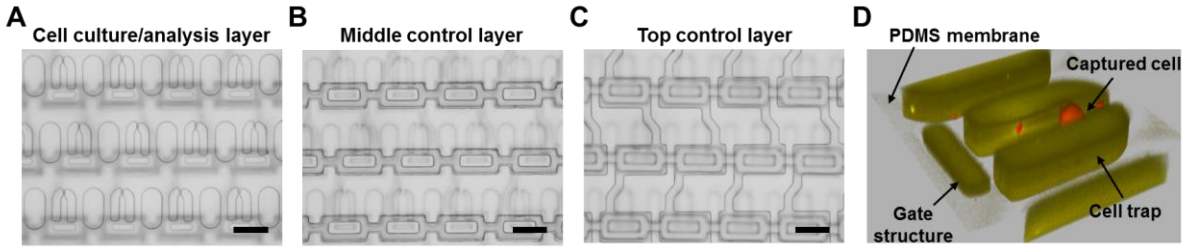


**SI Fig. S1.** Microfabricated high-throughput screening platform. (A-C) Microscopic images of each PDMS layer. (D) 3D reconstruction of the PDMS cell culture/analysis layer having a single *C. reinhardtii* cell captured within, visualized by imaging its chlorophyll autofluorescence. Scale bar = 100 μm.

**Numerical simulation of three different trapping site designs**

To estimate the trapping efficiency and backflow required to release cells, fluidic flow profiles inside the three different trapping sites were analyzed and compared through numerical simulation (SI Fig. S2; X ~ X': along the flow direction, Y ~ Y': across the center of a gap at each trap design). 3D schematics of each trapping structure design utilized in the simulation are shown in SI Fig. S2A, each having a different gap geometry; the first design has a bottom opening (cross section = 10 (width) x 3 (height) = 30 $\mu m^2$), the second design has a bottom opening with supporting structures (cross section = 10 x 3 = 30 $\mu m^2$), and the third design has a narrow gap in the center (cross section = 3 x 16 = 48 $\mu m^2$). Compared to the flow profiles before capturing a cell (SI Fig. S2B), flow speeds inside the trapping structures were decreased after capturing a cell, which reduces the chance for other cells to be introduced and captured in the same trap (SI Fig. S2C). Although the variation of flow speeds in each trapping structure design (average speed difference across the gap cross-section before and after cell capture: first design: 0.78 → 0.67 mm/s, second design: 0.72 → 0.29 mm/s, third design: 0.46 → 0.27 mm/s) could provide some valuable information about each trap design itself, this parameter was not appropriate for comparing the three different trapping structure designs due to their different gap geometry. Even under a constant flow condition, fluidic speed flowing through a microchannel can vary depending on the microchannel geometry (*e.g.*, cross-section), and thus, another parameter covering both the flow speed and the gap geometry is needed, that is, flow rate.

Flow rate, defined as the amount of fluid passing through the gap cross-section per unit time ($m^3/s$), was calculated by multiplying the average flow speed across the gap cross-section and the area of the gap cross-section in each trap design (SI Fig. S2E). Flow rate provides the volume of fluid flowing through each trap design regardless of gap sizes, which allows for side-by-side comparison of the three different trap designs. Before capturing cells, all three trapping structure designs had almost the same amount of fluid flowing inside. After capturing cells, 60% (first design), 14% (second design), and 40% (third design) of fluid flow was blocked with a captured cell (flow rate difference before and after cell capture: first design: $2.17 \times 10^{-14}$ → $0.87 \times 10^{-14}$ $m^3/s$, second design: $2.33 \times 10^{-14}$ → $2.02 \times 10^{-14}$ $m^3/s$, third design: $2.19 \times 10^{-14}$ → $1.31 \times 10^{-14}$ $m^3/s$). Based on these flow rate changes, the first design would have the highest single-cell trapping efficiency as less amount of fluid will flow through this trap design once the trapping sites are occupied, compared to the other two

designs, resulting in the least probability in capturing more than two cells in a single trap. The second design showed the smallest reduction in fluid volume after capturing a cell (only 14% decrease). This would mainly come from the supporting structures having a narrower channel width, resulting in space between a captured cell and the gap of the trap through which most of fluid can still flow.

Next, fluid flow during the cell extraction process (*i.e.*, when applying backflow to release cells) was analyzed through the three different trap designs with a captured cell inside (SI Fig. S2D). The highest flow rate and the lowest flow rate were observed from the second and the first designs, respectively, meaning that more backpressure will be needed for the first design to achieve the same degree of backflow compared to the other two designs. For example, approximately 2.3 and 1.5-fold of backflow is required in the first design to obtain the same amount of fluid flow as the second and the third designs (flow rate in the first design: $0.87 \times 10^{-14}$ $m^3/s$, flow rate in the second design: $1.96 \times 10^{-14}$ $m^3/s$, flow rate in the third design: $1.30 \times 10^{-14}$ $m^3/s$). Based on these simulation results, the first design will have the highest single-cell trapping efficiency, but will require more backflow during the cell extraction process. The second design will need the least backflow to release cells from the cell trap, but will have the lowest single-cell trapping efficiency. The third design will have a slightly lower trapping efficiency compared to the first design, but will require much less backflow to extract the cells for off-chip analysis. Considering these simulation results, the third trapping design was selected and utilized in the microfluidic single-cell screening platform.

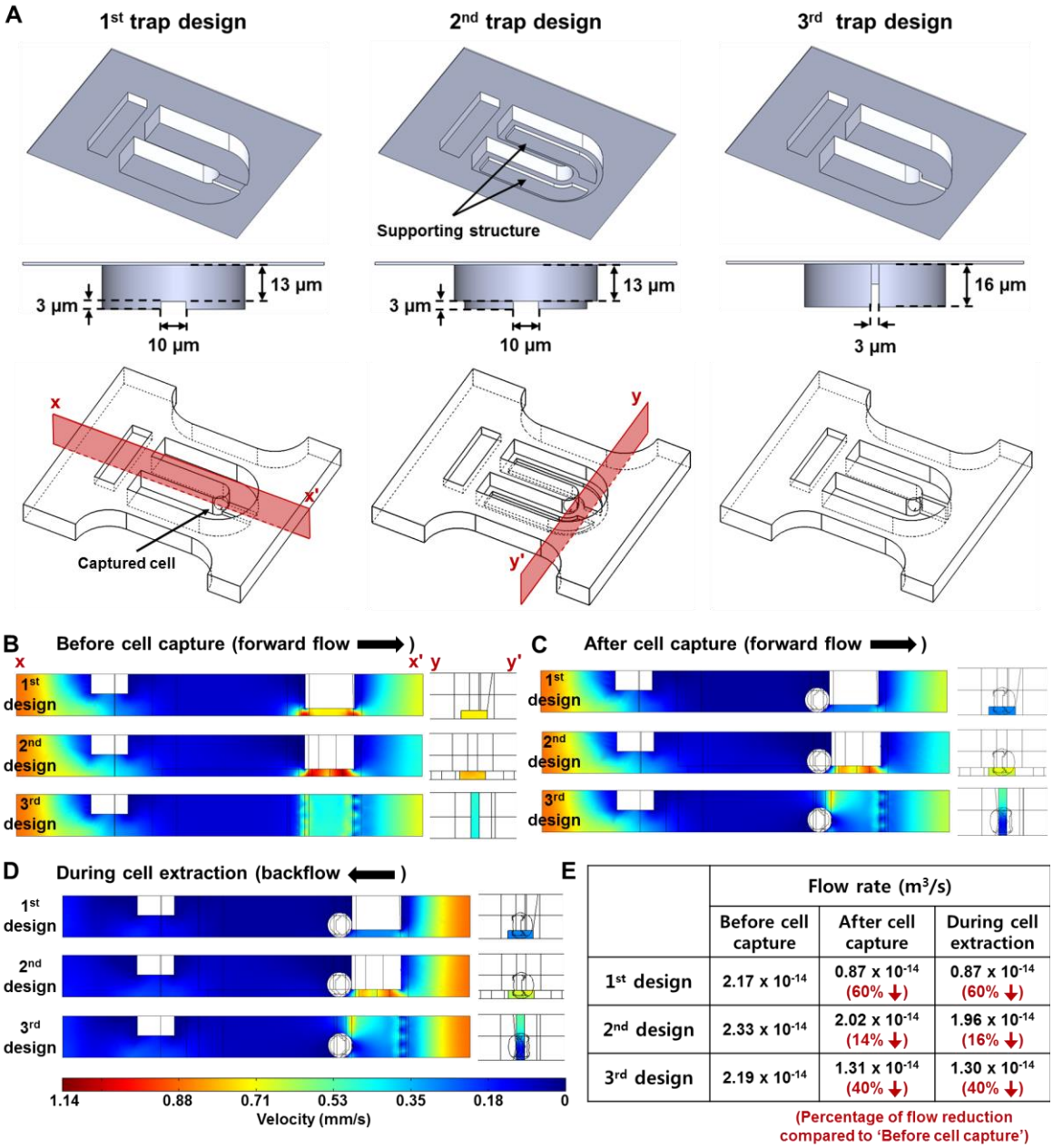


E

| | Flow rate ($m^3/s$) | | |
|---|---|---|---|
| | Before cell capture | After cell capture | During cell extraction |
| 1st design | $2.17 \times 10^{-14}$ | $0.87 \times 10^{-14}$ (60% ↓) | $0.87 \times 10^{-14}$ (60% ↓) |
| 2nd design | $2.33 \times 10^{-14}$ | $2.02 \times 10^{-14}$ (14% ↓) | $1.96 \times 10^{-14}$ (16% ↓) |
| 3rd design | $2.19 \times 10^{-14}$ | $1.31 \times 10^{-14}$ (40% ↓) | $1.30 \times 10^{-14}$ (40% ↓) |

(Percentage of flow reduction compared to 'Before cell capture')

**SI Fig. S2.** Numerical simulation results of the fluidic flow profiles of the three different trapping structure designs. (A) 3D illustrations of the first, second, and third trapping structure designs having three different gap geometries. Flow profiles of the three different trap designs analyzed along the flow direction as well as across the center of a gap (B) before capturing a cell, (C) after capturing a cell, and (D) during the cell extraction process (when backflow is applied). (E) Analysis of flow rate, the amount of fluid flow across the cross-section of a gap for each trap design.

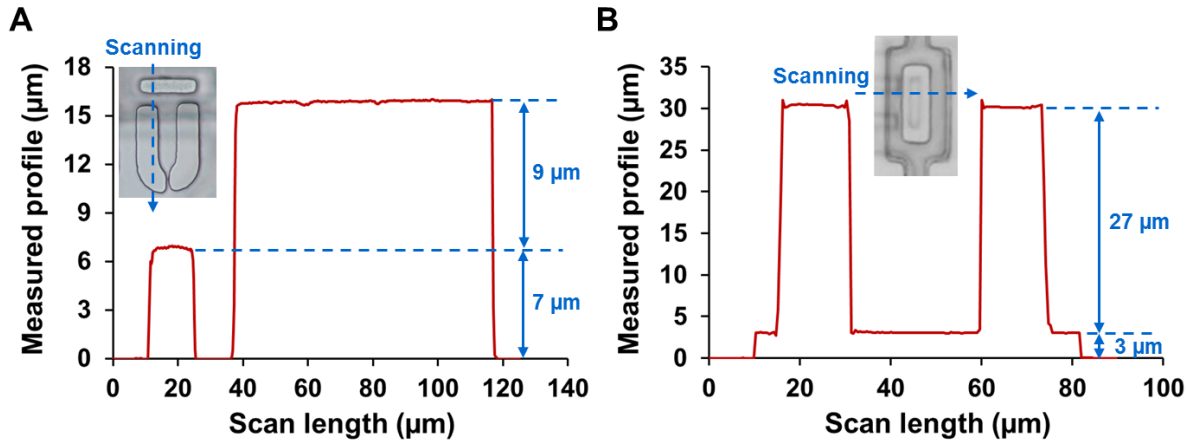


**Supplementary Fig. S1.** Thicknesses of (A) the fabricated cell culture/analysis layer consisting of the cell trap and the gate structure and (B) the middle control layer with the ridge structure, measured by an optical surface profilometer.

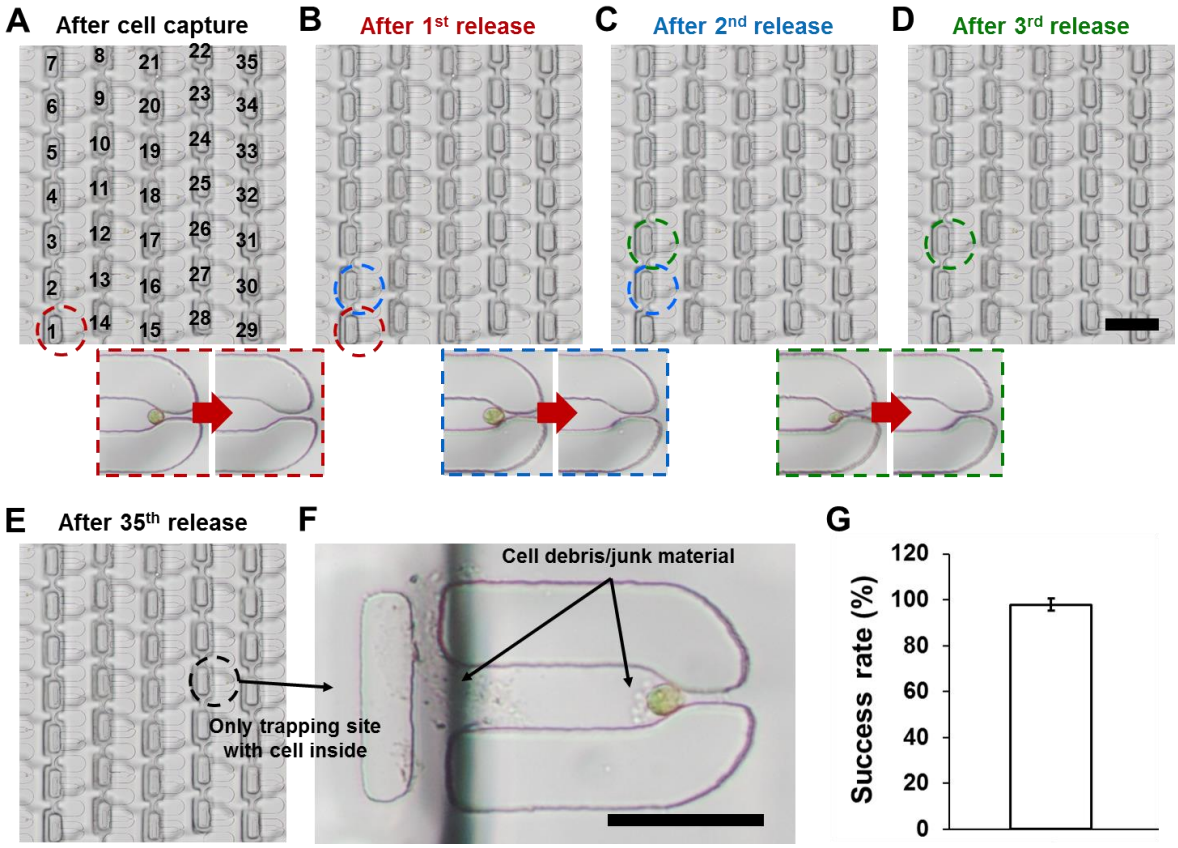


**Supplementary Fig. S2.** Success rate of the selective cell extraction process. (A-D) Microscopic images showing sequential retrieval of targeted cells (from 1st to 35th trapping sites). Insets show enlarged images of each trapping sites (*e.g.*, 1st, 2nd, and 3rd trapping sites) before and after the extraction process. Scale bar = 200 µm. (E) Microscopic image after the 35th selective extraction process, where *C. reinhardtii* cells captured at all trapping sites (1st ~ 35th) were successfully released and collected to an off-chip reservoir except the cell from the 25th trapping site. (F) Enlarged microscopic image of the 25th trapping site showing a *C. reinhardtii* cell with sticky cell debris and junk material, which were stuck to the PDMS device. Scale bar = 50 µm. (G) Analysis of successful cell extraction process in the platform (97.9 ± 2.7%, $n = 4$).

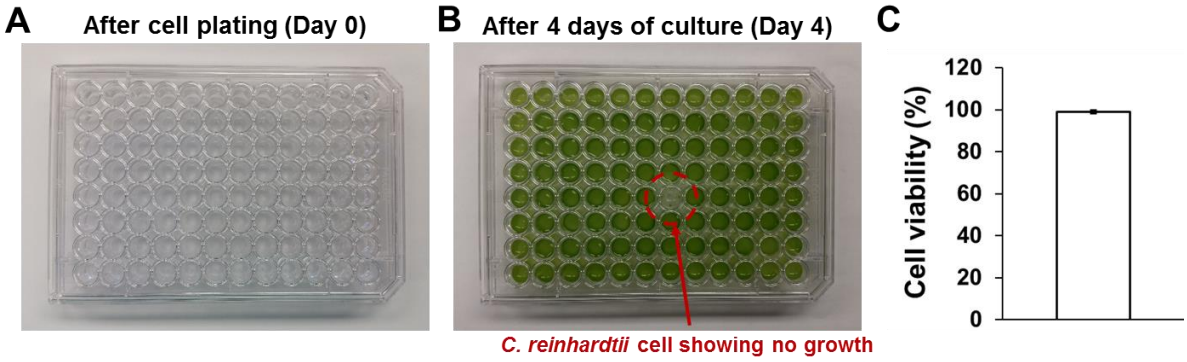


**Supplementary Fig. S3.** Cell viability test after the selective cell extraction process. (A-B) Images showing a 96-well culture plate after plating single retrieved *C. reinhardtii* cells into each well and after culturing them for 4 days. In this particular example, all cells showed viability and growth (doubling time: 6 ~ 8 hours) except for one culture well (highlighted with a red dashed circle). (C) Analysis of cell viability test (98.9 ± 0.9%, $n = 4$).

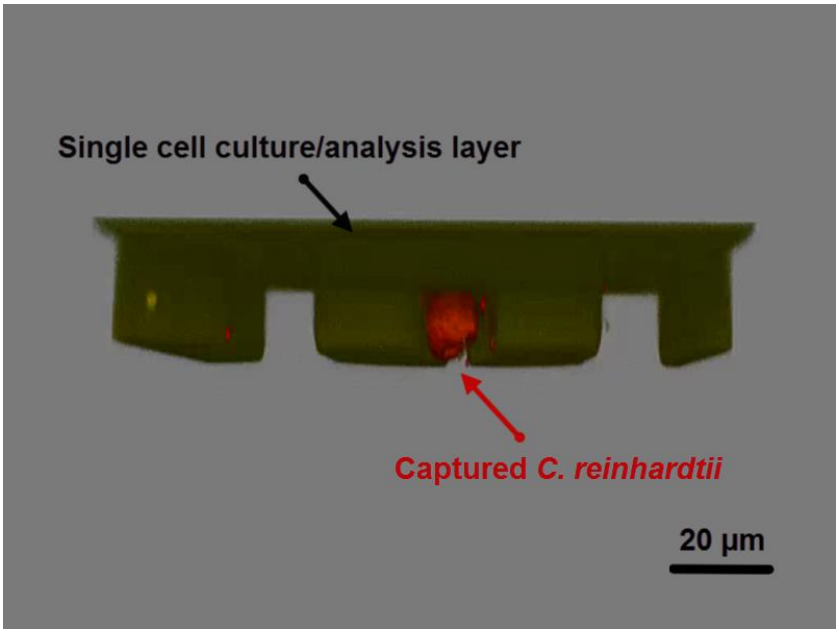


**Supplementary Video S1.** 3D structure of a single trapping site with a captured *C. reinhardtii*, reconstructed by confocal microscopy (yellow: Nile red stained PDMS device, red: chlorophyll autofluorescence of *C. reinhardtii*).

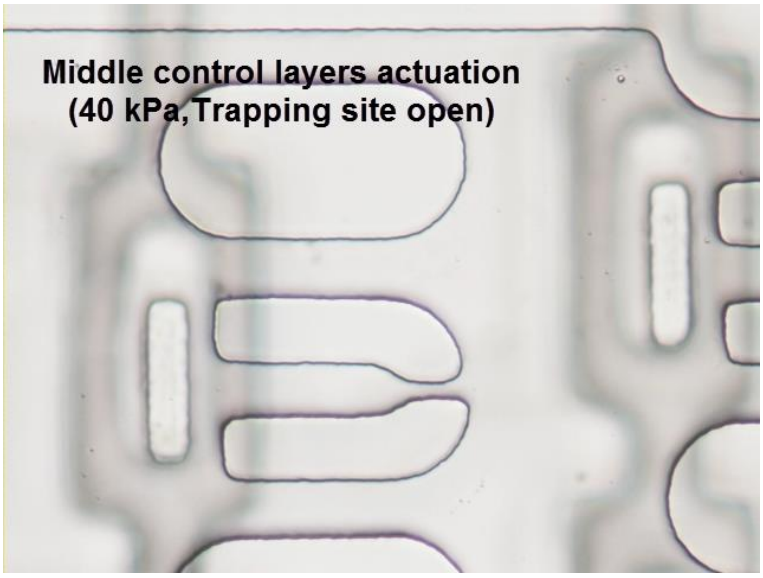


**Supplementary Video S2.** Operation of the microfluidic OR logic gate (middle control layer actuation only).

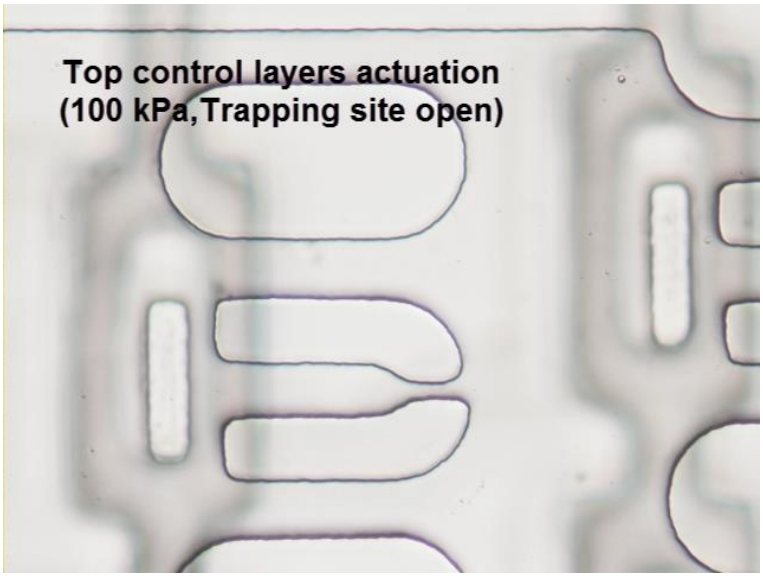


**Supplementary Video S3.** Operation of the microfluidic OR logic gate (top control layer actuation only).

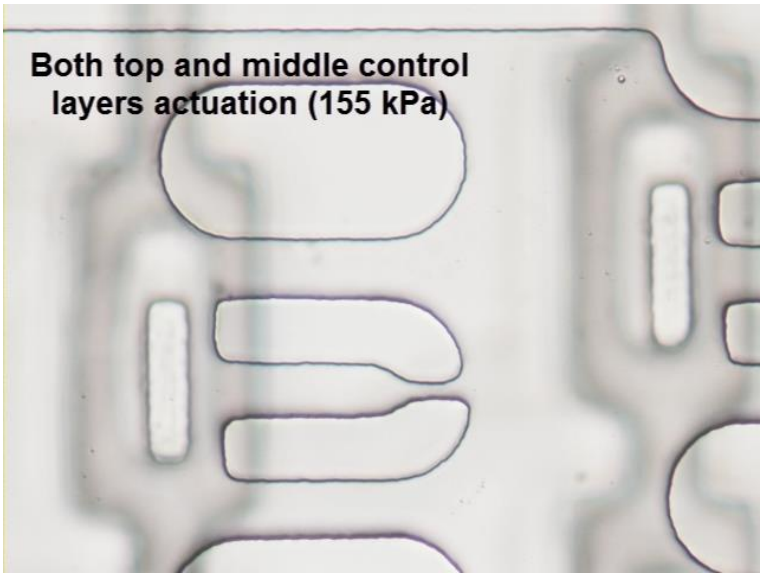


**Supplementary Video S4.** Operation of the microfluidic OR logic gate (both the top and middle control layers being actuated).

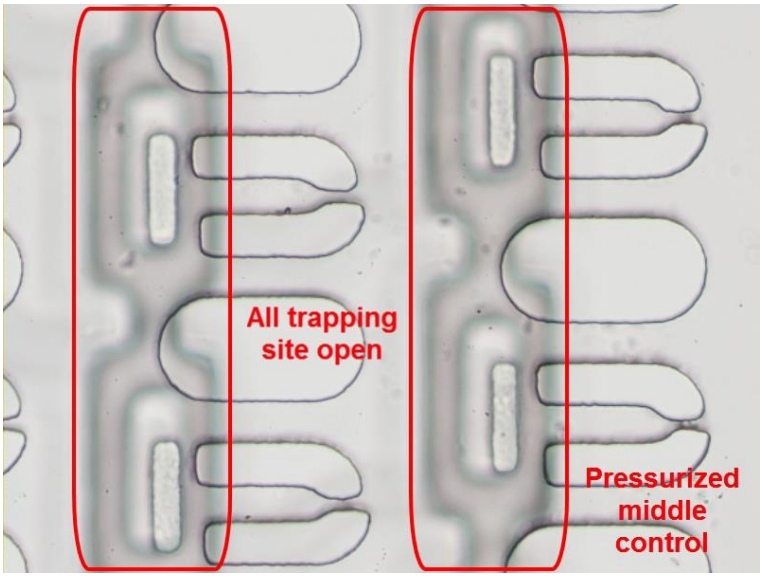


**Supplementary Video S5.** Operation of the microfluidic OR logic gate, showing the selection of a particular trapping site (in this case, the left bottom trapping site first, followed by the right top trapping site) from a 2 x 2 array trapping array.

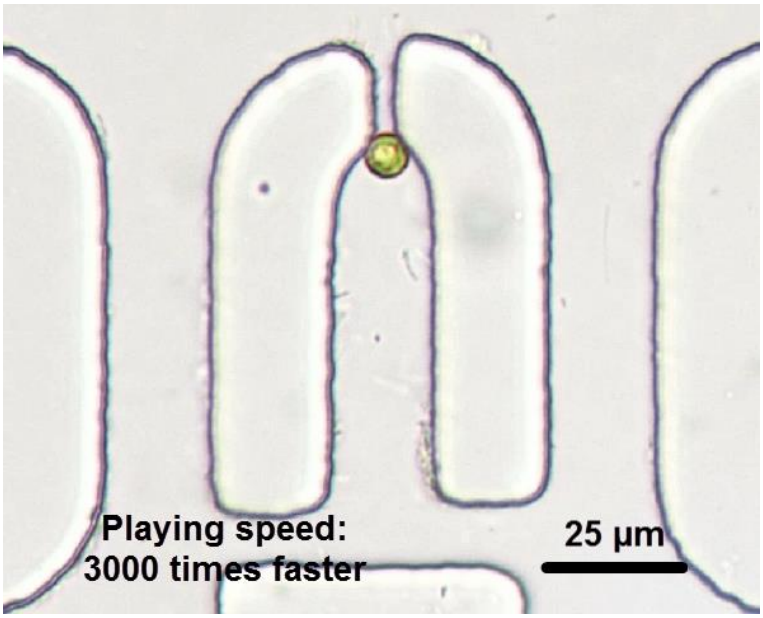


**Supplementary Video S6.** Time-course analysis of a single *C. reinhardtii* cell growth inside a trapping site of the microfluidic platform.

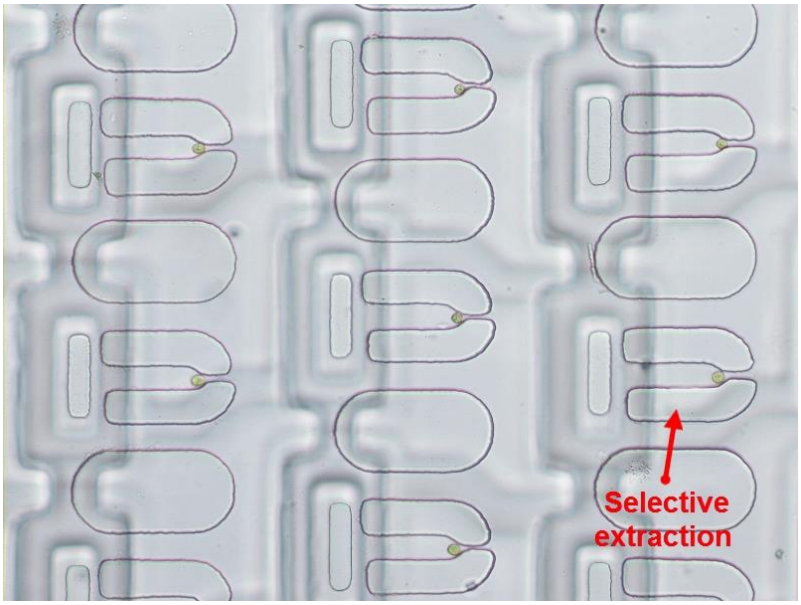


**Supplementary Video S7.** Sequential selective cell extractions from three different trapping sites.